Korean J. Chem. Eng., 40(10), 2520-2528 (2023)
DOI: 10.1007/s11814-023-1462-7

pISSN: 0256-1115
eISSN: 1975-7220

Fluoride-incorporated ionic clathrate hydrates

Byeonggwan Lee*, and Kyuchul Shin*,***,†**

*Department of Hydrogen & Renewable Energy, Kyungpook National University, 80 Daehak-ro, Buk-gu, Daegu 41566, Korea
**Korea Atomic Energy Research Institute, 111 Daedeok-daero 989, Yuseong-gu, Daejeon 34057, Korea
***Department of Applied Chemistry, Kyungpook National University, 80 Daehak-ro, Buk-gu, Daegu 41566, Korea
(*Received 20 February 2023 • Revised 27 March 2023 • Accepted 31 March 2023*)

Abstract−Ionic clathrate hydrates are promising materials for hydrate-based gas storage and separation processes. Here, we demonstrated that the hydroxide ion in the cubic structure-II (CS-II) and hexagonal structure-III (HS-III) ionic clathrate hydrates can be replaced by fluoride. Me_4N^+ and $Et_2Me_2N^+$ cations were selected as guest species for the CS-II and HS-III hydrates, respectively. The crystal structure of each hydrate was identified through Rietveld analysis of the PXRD pattern. The $Fd\bar{3}m$ structure (CS-II) of Me_4NF+N_2 or O_2 hydrates and the *P6/mmm* structure (HS-III) of $Et_2Me_2NF+CH_4$ hydrate were confirmed. We also investigated the phase equilibria of hydroxide or fluoride-incorporated CS-II and HS-III hydrate systems, and found that incorporating fluoride destabilizes the hydrate lattice to a greater extent than hydroxide. The present findings will provide better understanding of the guest-host interactions in ionic clathrate hydrates, and suggest their potential for practical applications in gas storage and separation technologies.

Keywords: Ionic Clathrate Hydrate, Gas Storage, Fluoride, Powder X-ray Diffraction, Inclusion Compound

INTRODUCTION

As a large class of solid inclusion compounds, clathrate hydrates can be classified into three types: canonical clathrate hydrates, semiclathrate hydrates, and ionic clathrate hydrates [1,2]. "Canonical" clathrate hydrates are those that neutral guest molecules are encaged in a neural host framework without permanent bonds between guest and host. Hydrates of rare gases, small gaseous molecules, or hydrocarbons which contain van der Waals interactions [1-3], weak hydrogen bonding [1,4,5], and halogen bonding [1,6-8] between the guest molecules and the host framework belong to this category.

Semiclathrate hydrates are those that neutral guest molecules are encaged in the framework but with permanent guest-host hydrogen bonding. Hydrates of various amines form these semiclathrates with numerous structural motifs [1,2,9]. Ionic clathrate hydrates are those in which cations or anions are encaged in the host lattice with counterions [1,10]. These hydrates are stabilized by the strong ionic interactions between ionic guest molecules and counterion-doped host lattice, as well as the guest-host van der Waals interaction.

Ionic clathrate hydrates can be further classified into three categories based on the type of ionic guest they contain. The first category comprises hydrates of strong acids, such as HPF_6, HBF_4, or $HClO_4$, in which anions such as PF_6^-, BF_4^-, or ClO_4^- are encaged in the protonated water lattice [10-17]. For HPF_6, the framework of the clathrate was reported to include hydrogen fluoride as well [12,13]. The second category comprises the hydrates of strong bases. The most well-known example of these materials is the hydrate of tetramethylammonium hydroxide (Me_4NOH), in which the Me_4N^+ cation is encaged in the OH^- incorporated water framework [10, 18-26]. The third category is the hydrate of quaternary alkyl ammonium or alkyl phosphonium salts [1,2,10,27-35]. In these hydrates, a large cation such as tetra-n-butyl ammonium (n-Bu_4N^+) or tetra-i-amyl ammonium (i-Am_4N^+) is encaged in a super-cage which is united with the truncated small cages. The counterion, commonly halide anions such as fluoride, chloride, or bromide and other anions such as hydroxide, borohydride, glycolate, and others, replaces one or two water molecules of the host framework [1,10,27-35]. The size of the anion incorporated in the lattice of these hydrates strongly affects the thermodynamic stability of clathrate structure [10, 36]. Nakayama and Torigata reported that the melting points of n-Bu_4N^+ hydrates are inversely proportional to the partial molar volume of monovalent counter-anions incorporated in the lattice framework [36]. The melting points of n-Bu_4N^+ hydrates with OH^- or F^-, which are the smallest anions for the quaternary alkyl ammonium salt hydrates, are higher than 298 K, while those with BrO_3^- or ClO_3^- are near 273 K [36]. This implies that the framework distortion caused by the incorporated anion destabilizes the clathrate structure of ionic hydrates.

Additionally, as a new type of ion-incorporated clathrate hydrate, NH_4F-doped clathrate hydrates have recently been reported [37-42]. The crystal structure of NH_4F solid is isostructural to hexagonal ice with a similar hydrogen bond length [43-45]. Therefore, the NH_4F-H_2O solid solution host lattice can replace not only the usual water host lattice of canonical clathrate hydrates, but also the clathrates of unusual guest molecules such as methanol or diol [37-41]. In these materials, the NH_4^+ and F^- ion pair substitutes two water molecules in the host framework, and the lattice dimension decreases slightly because the hydrogen bond length of NH_4F is slightly shorter than that between water molecules [45].

As stated above, the hydrates of strong bases are those that the cations are enclathrated in the OH^--doped host lattice. Me_4NOH has three clathrate hydrate structures depending on its hydration

†To whom correspondence should be addressed.
E-mail: kyuchul.shin@knu.ac.kr

number and temperature [18]. The first is the pentahydrate of Me_4NOH, which shows a cubic *Im-3m* structure with two $4^6 6^8$ cages in the unit cell in the temperature range between 42 to 68 °C. The second is the 7.5 hydrate of Me_4NOH, which shows a tetragonal *I4/mcm* structure with eight $5^{12}6^3$ cages and four vacant $4^2 5^8$ cages in the unit cell in the temperature range of 6 to 16 °C. The third is the decahydrate of Me_4NOH, which shows an orthorhombic *Pmna* structure with four $4^1 5^{10} 6^6$ cages and four vacant $4^3 5^6$ cages in the unit cell below −20 °C. These three Me_4NOH clathrate hydrates do not need the presence of secondary small guest molecules. Choi et al. reported that Me_4NOH can form a cubic structure II (CS-II) with $Fd\bar{3}m$ space group in the presence of methane or hydrogen molecules as secondary guests [19]. In these binary hydrates, Me_4N^+ ions occupy the large $5^{12}6^4$ cages and small molecules such as CH_4, H_2, N_2, or O_2 occupy the small 5^{12} cages in the CS-II hydrates [19,21-26]. Another example of a hydroxide-doped clathrate hydrate that forms in the presence of secondary guest molecule is diethyldimethylammonium hydroxide (Et_2Me_2NOH) [46]. Et_2Me_2NOH does not form a clathrate structure by itself, but pressurizing Et_2Me_2NOH aqueous solution with help gas such as methane or xenon induces the formation of binary clathrate hydrate of hexagonal structure III (HS-III), also known as structure H (sH) hydrate, with *P6/mmm* space group [1,46].

Because of their gas-storing ability, Me_4NOH and Et_2Me_2NOH can be utilized for the hydrate-based gas storage and separation processes. In addition, Ahn et al. reported that the N_2O molecule, one of the greenhouse gases, captured in Me_4NOH clathrate hydrate is decomposed into non-greenhouse gases of N_2 and O_2 by gamma-irradiation and they proposed the concept of clathrate nanocage reactor with dual functions in sequestration and treatment of greenhouse gases [26]. Ionic clathrate hydrates are applicable materials to many energy and environmental issues, thus further in-depth investigation is needed to understand the nature of guest-host interaction in those materials.

Herein, we demonstrate that the fluoride ion can replace the hydroxide in the hydrates of Me_4N^+ and $Et_2Me_2N^+$. Although it is known that fluoride can be incorporated in the framework of quaternary alkyl ammonium salt clathrate such as n-Bu_4NF or i-Am_4NF, which contains united super cages [1,10,27], there have been no reports of fluoride incorporation in conventional clathrate structures, such as cubic structure I (CS-I), CS-II, or HS-III, except for NH_4F ion pairs. In this study, we report the first fluoride-incorporated CS-II and HS-III ionic clathrate hydrates. The crystal structure of each clathrate was identified using powder X-ray diffraction (PXRD) pattern analysis. The phase equilibria of fluoride-incorporated hydrate systems were also investigated and compared to hydroxide-incorporated systems.

EXPERIMENTAL DETAILS

1. Sample Preparation

Tetramethylammonium hydroxide pentahydrate ($Me_4NOH{\cdot}5H_2O$, 98% purity) and tetra-methylammonium fluoride tetrahydrate ($Me_4NF{\cdot}4H_2O$, 98% purity) were purchased from Alfa Aesar. Diethyldimethyl-ammonium hydroxide solution (Et_2Me_2NOH, ~20% in H_2O) and hydrofluoric acid (HF, 48 wt% in H_2O) were purchased from Sigma-Aldrich. Methane gas of 99.95% purity and nitrogen and oxygen gases of 99.999% purity were supplied from Korea Standard Gas (Korea). Deionized water (LabWater PURELAB Q7, ELGA, Lane End, U.K.) with ultrahigh purity was used for the sample preparation.

Aqueous solutions of Me_4NOH, Me_4NF (5.88 mol%), and Et_2Me_2NOH (2.94 mol%) were prepared. Et_2Me_2NF solution (2.94 mol%, formal concentration) was prepared by mixing Et_2Me_2NOH and HF solutions. Because Et_2Me_2NOH is a strong base and the equilibrium constant of the neutralization reaction between OH^- and HF is large, it is believed that the acid-base neutralization reaction was complete. The solutions were well-mixed, reacted for a sufficient time, and degassed by a vacuum pump. Then, each solution was quenched drop by drop and finely powdered under liquid nitrogen temperature. The fine powder was placed into a precooled high-pressure vessel and pressurized with O_2 or N_2 (300 bar) for Me_4NX (X=OH or F) and CH_4 (70 bar) for Et_2Me_2NX (X=OH or F), respectively. The pressurized vessels were kept at 243 K for at least four days to maximize hydrate conversion. Then, the synthesized sample was collected and stored in a liquid nitrogen tank.

2. PXRD and Structural Analysis

The PXRD patterns were recorded at 100 K by an ADSC Quantum 210 CCD diffractometer with synchrotron radiation (λ= 0.9000 Å) on the supramolecular crystallography beamline (2D) at the Pohang Accelerator Laboratory (PAL) in Korea. A precooled polyimide tube (Cole-Parmer) filled with the sample was loaded into the equipment. The sample was finely powdered (~45 μm) before the measurement. Debye-Scherrer rings were recorded with a resolution of 4096 by 4096 pixels and converted into one-dimensional patterns of 2θ range from 0 to 67.4940°. The recording time for each sample was below 30 s so as to minimize the sample damage by synchrotron beam radiation.

The patterns obtained were refined by the previously reported structural analysis of clathrate hydrates [37,38,46,47]. The positions of guest molecules in the cages were determined by direct space methods using the FOX program [48]. The guest molecules were assumed to be rigid. Virtual species having the sums of atomic scattering factors were used for H_2O, CH_4, $-CH_3$, and $-CH_2-$ to include the contribution of hydrogen atoms on the diffraction pattern during the refinement [47]. Fluoride and hydroxide ions were not distinguishable from water in the host framework because of the similarity of their scattering factors. The FULLPROF program with the Rietveld analysis was used for the PXRD pattern refinement [49], and the crystal structures were visualized by the VESTA program [50].

3. Phase Equilibria Measurements

The L_W-H-V phase equilibria of binary Me_4NX+N_2 or O_2 and $Et_2Me_2NX+CH_4$ hydrates (X=OH, F) were determined using the isochoric P-T trace method. The strong bases, Me_4NOH and Et_2Me_2NOH solutions, can corrode rubber sealing rings and this can seriously lead to the wrong results of phase equilibria. Thus, we used a long cylindrical high-pressure vessel with a magnetic bar instead of a mechanical stirrer to avoid solution splashing and corrosion of sealing rings. Because magnetic bar stirring cannot assure vigorous hydrate formation, we first prepared the powder sample (~20 g) from the sample preparation process above and put it into the pre-

cooled vessel with a magnetic bar. The vessel was vacuumed at liquid nitrogen temperature, and the precooled N_2, O_2, or CH_4 gas was slowly injected into the vessel as the temperature gradually increased. After the system reached the target pressure and temperature and stabilized, the vessel was slowly warmed at a rate of 0.1 K/h. The temperature and pressure inside the vessel were measured by a resistance temperature detector and a pressure transducer with uncertainties of ±0.05 K and ±0.005 MPa, respectively, and were continuously monitored and recorded by a data acquisition system. The phase boundary point was determined to be where the slope of the tangent line of the dissociation curve suddenly changed.

RESULTS AND DISCUSSION

The crystal structures of binary Me_4NOH+N_2, Me_4NOH+O_2, and $Et_2Me_2NOH+CH_4$ clathrate hydrates are known to the CS-II for the first two and the HS-III for the last one [23,46]. The crystal radii of F^- and OH^- (calculated from X-ray data of their crystals with many cations) are 1.17 Å and 1.21 Å (for coordination number 4), respectively, whereas those of Cl^- and Br^- are 1.67 Å and 1.82 Å (for coordination number 6) [51]. The conventional partial molar volume of ions in aqueous solution, which is obtained at infinite dilution and with setting the value of H^+ is zero at all temperatures, is −1.16 cm^3/mol for F^-, −4.04 cm^3/mol for OH^-, 17.83 cm^3/mol for Cl^-, and 24.71 cm^3/mol for Br^- at 25 °C [36, 52]. The absolute partial molar volumes of ions in an aqueous solution can be calculated by $V^{\infty}(ion)=V^{conv}(ion)+zV^{\infty}(H^+, aq)$, where $V^{\infty}(ion)$ is the absolute partial molar volume of an ion, $V^{conv}(ion)$ is the conventional partial molar volume of an ion, $V^{\infty}(H^+, aq)$ is the absolute value for H^+, and z is the charge number of the ion [52-54]. Marcus reported that the absolute values for F^-, OH^-, Cl^-, and Br^- are calculated to be 4.25, 1.2, 23.24, and 30.12 cm^3/mol at 25 °C, respectively [53,54]. From the crystal radii and the standard partial molar volumes of ions, it is expected that the filling space of F^- in the hydrate lattice and the distortion degree of lattice caused by its incorporation is similar to those of OH^-. Indeed, for the clathrate hydrates of n-$Bu_4N^+X^-$ salts, the melting points of the hydrates for fluoride and hydroxide anions are similar to each other and quite higher than those of chloride or bromide anions [35,36]. Therefore, the hydroxide in the clathrate hydrates of Me_4N^+ or $Et_2Me_2N^+$ cations might also be replaced by the fluoride anion.

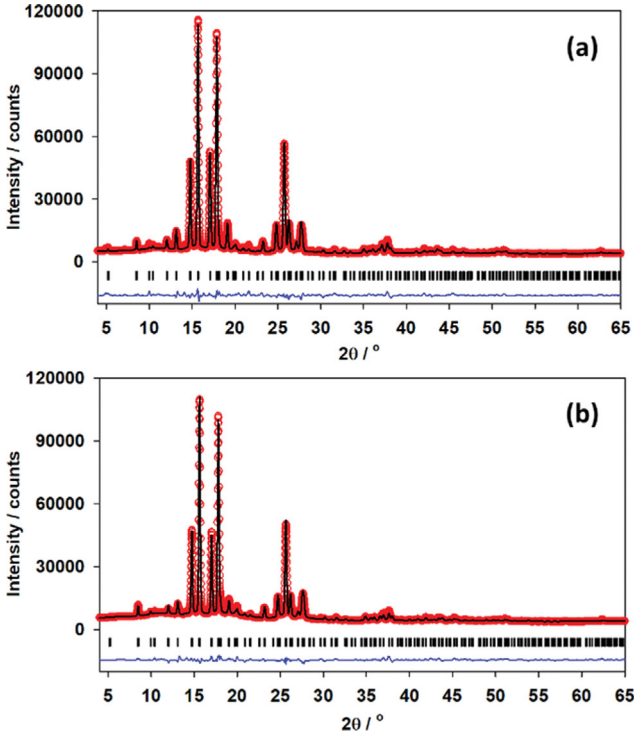

Fig. 1. PXRD patterns of (a) Me_4NOH+O_2 and (b) Me_4NF+O_2 clathrate hydrates. Space group and lattice parameters: (a) *Fd-3m*, a=17.1302(7) Å, (b) *Fd-3m*, a=17.2125(6) Å. Reliability factors (background corrected): (a) χ^2=20.2, R_{wp}=12.3%, (b) χ^2=11.9, R_{wp}=10.7%.

To determine whether the fluoride is indeed able to replace the role of OH^- in the ionic clathrate hydrates, the binary Me_4NF+O_2 or N_2 hydrates were synthesized, and their crystal structures were investigated. Fig. 1 shows the PXRD patterns of binary Me_4NOH or Me_4NF+O_2 hydrates and their Rietveld refinement results. The atomic coordinates, site occupancies, and isotropic temperature factors are also given in Tables 1 and 2. As shown in Fig. 1, both PXRD patterns show only one solid phase with the space group of $Fd\bar{3}m$ and the lattice parameters of a=17.1302(7) Å for Me_4NOH+

Table 1. The coordinates of host molecules and guest atoms (or atomic groups), isotropic temperature factors, and site occupancies for the CS-II Me_4NOH+O_2 clathrate hydrate

Group	x	y	z	B (Å^2)	g	Site
Wa1	0.125	0.125	0.125	3.8(1)	1	8a
Wa2	0.2166(1)	0.2166	0.2166	3.2(1)	1	32e
Wa3	0.1852(1)	0.1852	0.3702(1)	5.6(1)	1	96g
O1	0.2238	0.0142	0.2355	0.01	0.1497(6)	96g
O2	0.2931	0.0239	0.2434	0.01	0.0748	192i
NL1	0.3984	0.3794	0.4092	8.6(4)	0.0417	192i
ML2	0.4533	0.4313	0.4543	8.6	0.0833	96g
ML3	0.3262	0.3644	0.4572	8.6	0.0417	192i
ML4	0.4382	0.3029	0.3914	8.6	0.0417	192i
ML5	0.3758	0.4191	0.3339	8.6	0.0417	192i

Table 2. The coordinates of host molecules and guest atoms (or atomic groups), isotropic temperature factors, and site occupancies for the CS-II Me_4NF+O_2 clathrate hydrate

Group	x	y	z	B (Å^2)	g	Site
Wa1	0.125	0.125	0.125	2.3(1)	1	8a
Wa2	0.2154(1)	0.2154	0.2154	3.5(1)	1	32e
Wa3	0.1860(1)	0.1860	0.3704(1)	6.9(1)	1	96g
O1	0.2574	1.0052	0.2906	0.1(1)	0.0833	192i
O2	0.2032	0.9888	0.2492	0.1(1)	0.0833	192i
NL1	0.3972	0.3556	0.3723	9.5(5)	0.0404(2)	192i
ML2	0.4164	0.3373	0.2889	9.5	0.0404	192i
ML3	0.3340	0.4163	0.3751	9.5	0.0809	96g
ML4	0.4687	0.3861	0.4127	9.5	0.0404	192i
ML5	0.3695	0.2829	0.4125	9.5	0.0404	192i

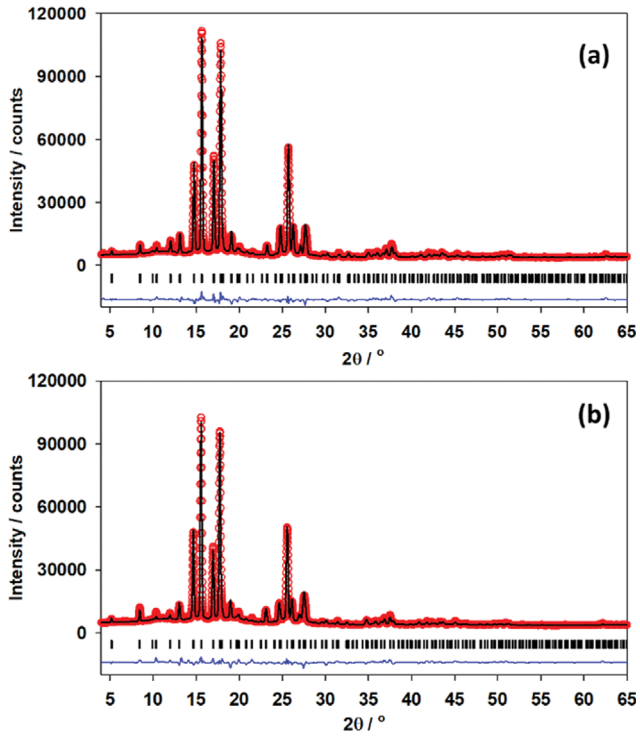

Fig. 2. PXRD patterns of (a) Me_4NOH+N_2 and (b) Me_4NF+N_2 clathrate hydrates. Space group and lattice parameters: (a) *Fd-3m*, a=17.1600(6) Å, (b) *Fd-3m*, a=17.2536(8) Å. Reliability factors (background corrected): (a) χ^2=15.4, R_{wp}=11.1%, (b) χ^2=17.8, R_{wp}=12.9%.

O_2 hydrate and a=17.2125(6) Å for Me_4NF+O_2 hydrate, respectively. Fig. 2 shows the PXRD patterns of binary Me_4NOH or Me_4NF+N_2 hydrates. The atomic coordinates, site occupancies, and isotropic temperature factors obtained from the Rietveld analysis are tabulated in Tables 3 and 4. In Fig. 2, both patterns also show $Fd\bar{3}m$ phase only, with the lattice parameters of a=17.1600(6) Å for Me_4NOH+N_2 hydrate and a=17.2536(8) Å for Me_4NF+N_2 hydrate, respectively. All lattice parameter values of the patterns in Fig. 1 and 2 agree with the literature for typical CS-II hydrate [1-3]; thus, it is concluded that fluoride can replace hydroxide in the CS-II ionic clathrate hydrates. For both O_2 and N_2, the fluoride-incorporated hydrates have slightly larger lattice parameter values than the hydroxide-incorporated ones, although the bond radius of fluoride 4-coordinated in the crystal lattice is slightly smaller than that of hydroxide [51]. One plausible explanation is that the space occupied by fluoride in the lattice is slightly larger because of the larger partial molar volume of fluoride ion surrounded by water molecules than hydroxide with the same situation [52-54]. The difference in H_2O-F^- and H_2O-OH^- hydrogen bonding interactions also could lead to the larger lattice parameters of fluoride-incorporated hydrates. In Fig. 3, the positions of guest molecules with full symmetry in the cages obtained from the Rietveld refinements of Me_4NX hydrates are shown, and there is not a remarkable difference in the guest behavior between Me_4NOH and Me_4NF hydrates (Fig. 3). The anion effect on the guest-host interactions in ionic clathrate hydrates could be minor.

As the next step, we also examined whether fluoride can replace the hydroxide in the HS-III clathrate hydrates. The binary $Et_2Me_2NF+CH_4$ hydrate was synthesized and the crystal structure was investigated by Rietveld analysis. Fig. 4 and Table 5 show the PXRD pattern of $Et_2Me_2NF+CH_4$ hydrate and its Rietveld refinement results. As seen in Fig. 4, the pattern shows a *P6/mmm* structure with the lattice parameters of a=12.1103(8) and c=10.0479(7) Å with a small amount of hexagonal ice impurity. The space group and lattice parameters are in good agreement with the literature for typical HS-III hydrates [1-3]. Therefore, it was confirmed that fluoride can also be incorporated in the ionic HS-III hydrates as well as CS-II hydrates. The previous study reported that the lattice parameters of $Et_2Me_2NOH+CH_4$ hydrates are a=12.109(3) and c=10.074(3) Å at 153 K [46]. The PXRD patterns in this work were recorded at 100 K. Considering the recording temperatures in the previous and present studies, it is thought that the lattice parameters of the fluoride-incorporated HS-III hydrate are larger than those of the hydroxide-incorporated one, as well as the case of CS-II hydrates. Fig. 4(b) represents the crystal structure of $Et_2Me_2NF+CH_4$ clathrate hydrate with full symmetry of guest molecules. The long chain of $Et_2Me_2N^+$ ion is located along the long axis of a large icosahedral ($5^{12}6^8$) cage, and methane molecules occupy the regular (5^{12}) and irregular ($4^35^66^3$) dodecahedral cages at slightly off-centered positions (Fig. 4(b)).

Table 3. The coordinates of host molecules and guest atoms (or atomic groups), isotropic temperature factors, and site occupancies for the CS-II Me_4NOH+N_2 clathrate hydrate

Group	x	y	z	B (Å^2)	g	Site
Wa1	0.125	0.125	0.125	2.5(1)	1	8a
Wa2	0.2174(1)	0.2174	0.2174	3.1(1)	1	32e
Wa3	0.1853(1)	0.1853	0.3703(1)	5.6(1)	1	96g
N1	1.0160	0.5272	0.4608	0.01	0.0833	192i
N2	0.9823	0.4802	0.4878	0.01	0.0833	192i
NL1	0.6266	0.6250	0.5840	5.8(3)	0.0417	192i
ML2	0.6212	0.6712	0.6584	5.8	0.0417	192i
ML3	0.6784	0.5551	0.5965	5.8	0.0417	192i
ML4	0.6604	0.6755	0.5205	5.8	0.0417	192i
ML5	0.5463	0.5979	0.5605	5.8	0.0417	192i

Table 4. The coordinates of host molecules and guest atoms (or atomic groups), and site occupancies for the CS-II Me_4NF+N_2 clathrate hydrate

Group	x	y	z	B (Å^2)	g	Site
Wa1	0.125	0.125	0.125	2.5(1)	1	8a
Wa2	0.2157(1)	0.2157	0.2157	2.8(1)	1	32e
Wa3	0.1879(1)	0.1879	0.3705(1)	8.0(1)	1	96g
N1	0.7661	0.2617	0.4816	1.6(2)	0.0833	192i
N2	0.7042	0.2684	0.4941	1.6	0.0833	192i
NL1	0.8604	0.8994	0.3499	13.8(4)	0.0417	192i
ML2	0.8709	0.8321	0.2952	13.8	0.0417	192i
ML3	0.8106	0.9603	0.3120	13.8	0.0417	96g
ML4	0.9386	0.9335	0.3693	13.8	0.0417	192i
ML5	0.8216	0.8716	0.4231	13.8	0.0417	192i

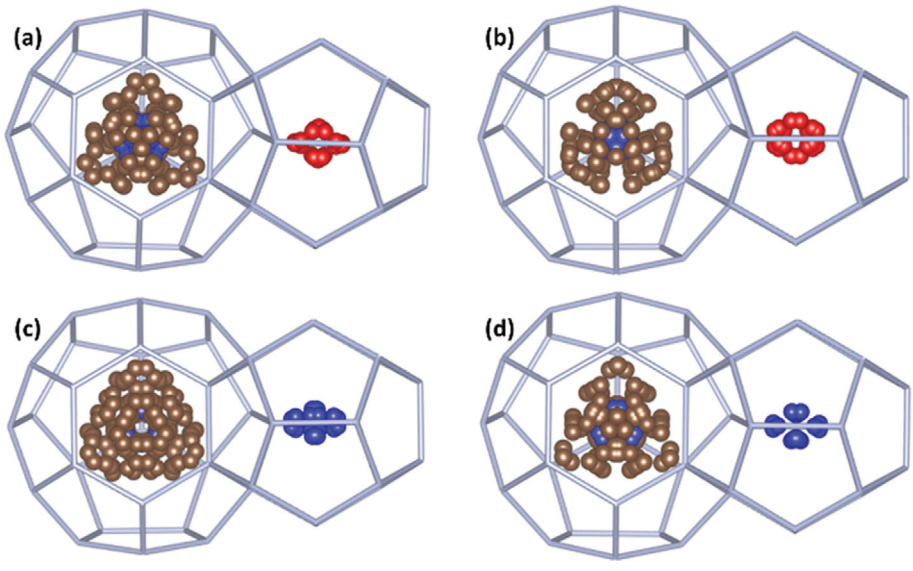

Fig. 3. Guest molecules with all symmetry-equivalent positions obtained from the Rietveld refinements. (a) Me_4NOH+O_2, (b) Me_4NF+O_2, (c) Me_4NOH+N_2, (d) Me_4NF+N_2 clathrate hydrates (brown: carbon, blue: nitrogen, red: oxygen. Hydrogen atoms and host molecules are omitted).

PXRD pattern analysis confirmed that the fluoride ion can be incorporated in the clathrate framework as a counterion of cationic guest species. To investigate the thermodynamic stability of fluoride-incorporated ionic clathrate hydrates, we also measured the phase equilibria of binary Me_4NX+N_2 or O_2 and $Et_2Me_2NX+CH_4$ clathrate hydrates ($X=F^-$ or OH^-). The obtained data in this work

are shown in Fig. 5 and tabulated in Table 6. As seen in Fig. 5(a), the phase boundary curves of Me_4NOH+O_2 and N_2 hydrates are in the region of higher temperature and lower pressure than those of pure O_2 and N_2 hydrates, respectively [55-57]; therefore, Me_4NOH acts as a thermodynamic promoter that enhances thermodynamic

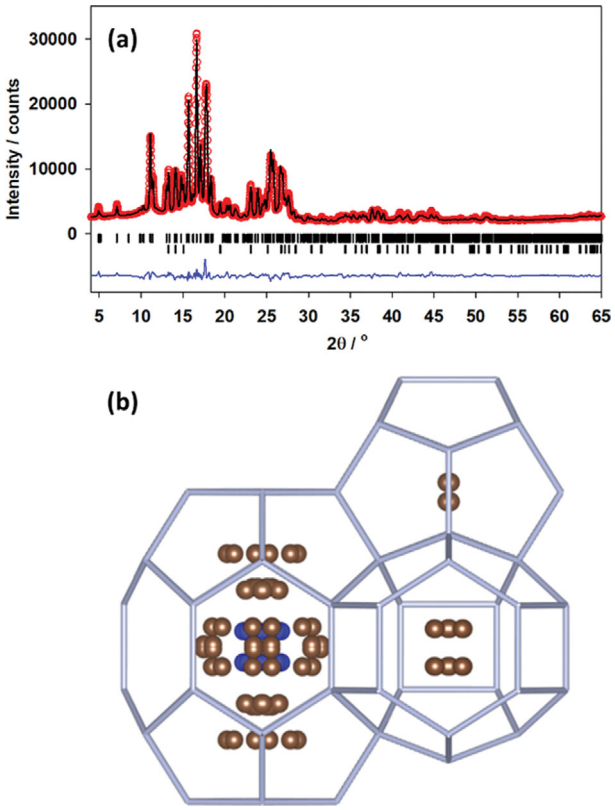

Fig. 4. (a) PXRD pattern of binary $Et_2Me_2NF+CH_4$ hydrate (the first row of Bragg ticks, space group: *P6/mmm*, lattice parameters: a=12.1103(8) and c=10.0479(7) Å, background corrected reliability factors: χ^2=7.62, R_{wp}=13.2%) with hexagonal ice (the second row of Bragg ticks, space group: *P6$_3$/mmc*, lattice parameters: a=4.4936(4) and c=7.3204(9) Å) (b) Guest molecules with all symmetry-equivalent positions obtained from the Rietveld refinements (brown: carbon, blue: nitrogen. Hydrogen atoms and host molecules are omitted).

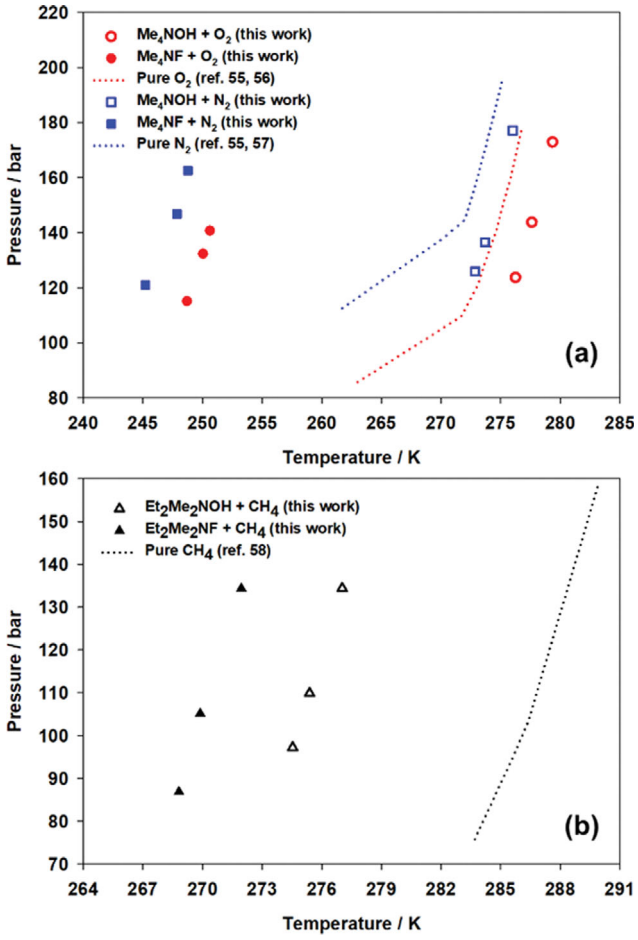

Fig. 5. Phase equilibrium curves of (a) Me_4NOH and Me_4NF with O_2 or N_2 and (b) Et_2Me_2NOH and Et_2Me_2NF with CH_4 clathrate hydrate systems [55-58].

Table 5. The coordinates of host molecules and guest atoms (or atomic groups), isotropic temperature factors, and site occupancies for the HS-III $Et_2Me_2NF+CH_4$ clathrate hydrate

Group	x	y	z	B (Å^2)	g	Site
Wa1	0.3333	0.6667	0.1350(4)	3.1(1)	1	4h
Wa2	0.1325(3)	0.2650	0	4.9(1)	1	6l
Wa3	0	0.3710(2)	0.3627(3)	8.3(1)	1	12n
Wa4	0.2089(2)	0.4178	0.2205(2)	3.8(1)	1	12o
CH_4(1)	0.7168	0.3611	0.5608	0.01	0.0752(8)	24r
CH_4(2)	0.0381	0.5143	0.0311	2.7(5)	0.1162(12)	24r
NL1	0.0203	0.0608	0.4496	15.0(6)	0.0417	24r
ML2	0.1197	0.1925	0.4932	15.0	0.0417	24r
ML3	0.0104	−0.0387	0.5510	15.0	0.0417	24r
ML4	0.0590	0.0272	0.3167	15.0	0.0417	24r
ML5	−0.1063	0.0549	0.4359	15.0	0.0417	24r
ML6	0.0749	0.1133	0.1993	15.0	0.0417	24r
ML7	−0.0270	−0.0252	0.6920	15.0	0.0417	24r

Table 6. Phase equilibrium data of Me_4NOH, Me_4NF, Et_2Me_2NOH, and Et_2Me_2NF clathrate hydrate systems

Me_4NOH+O_2		Me_4NF+O_2		Me_4NOH+N_2		Me_4NF+N_2		$Et_2Me_2NOH+CH_4$		$Et_2Me_2NF+CH_4$	
T/K	P/bar	T/K	P/bar	T/K	P/bar	T/K	P/bar	T/K	P/bar	T/K	P/bar
276.2	123.8	248.7	115.1	272.9	125.9	245.2	121.1	274.5	97.2	268.8	86.9
277.6	143.8	250.0	132.3	273.7	136.5	247.9	146.8	275.4	109.9	269.9	105.2
279.4	173.0	250.6	140.7	276.0	177.2	248.8	162.6	277.0	134.4	272.0	134.4

stability of binary hydrate compared to clathrate hydrate of pure O_2 or N_2 gases. On the other hand, as seen in Fig. 5(b), the Et_2Me_2NOH shifts the phase boundary curve to a lower-temperature and higher-pressure region than that of pure methane, that is, Et_2Me_2NOH acts as a thermodynamic inhibitor for methane hydrate. The difference in thermodynamic stability between Me_4NOH and Et_2Me_2NOH hydrates could be due to the difference in guest-host ionic interactions. It was reported that the hydroxide ion prefers to be located at the hexagonal faces of $5^{12}6^4$ cages in the CS-II Me_4NOH+O_2 hydrate [24,25]. Although the distribution of hydroxide in the HS-III $Et_2Me_2NOH+CH_4$ hydrate has not been investigated, it is expected that the hydroxide is similarly located at the hexagonal faces of $5^{12}6^8$ cages because of the weakness of hydrogen bonding

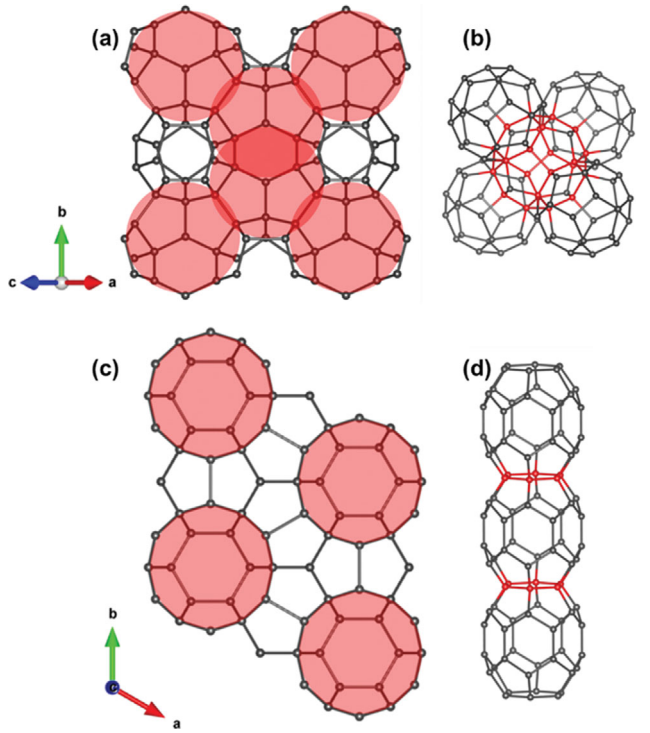

Fig. 6. (a) Crystal structure of CS-II hydrate with the view direction of (1 0 1) projection vector. The red shade region indicates the large $5^{12}6^4$ cages. (b) A $5^{12}6^4$ cage in the CS-II hydrate tetrahedrally connected with neighboring $5^{12}6^4$ cages. Red balls indicate the oxygens connecting two cages. (c) Crystal structure of HS-III hydrate with the view direction of (0 0 1) projection vector. The red shade region indicates the large $5^{12}6^8$ cages. (d) A $5^{12}6^8$ cage in the HS-III hydrate cylindrically connected with neighboring $5^{12}6^8$ cages. Red balls indicate the oxygens connecting two cages.

in the hexagonal rings of ~120° angle compared to the pentagonal rings of ~108° angle [1]. The center of $5^{12}6^4$ cage in the CS-II hydrate has $\bar{4}3m$ (T_d) symmetry [1] and the hexagonal faces of this cage are tetrahedrally located at the same distance apart from the center. Via these hexagonal faces, a $5^{12}6^4$ cage in the CS-II hydrate is tetrahedrally connected to four neighboring $5^{12}6^4$ cages (Fig. 6(a), 6(b)). On the other hand, the $5^{12}6^8$ cage in the HS-III hydrate has a cylindrical shape, and the symmetry of the cage center is 6/mmm (D_{6h}) [1]. This cage has eight hexagonal faces, two perpendicular and six parallel faces to the six-fold axis. A $5^{12}6^8$ cage in the HS-III hydrate is cylindrically connected to two neighboring $5^{12}6^8$ cages via perpendicular hexagonal faces, and each 'cylinder' of $5^{12}6^8$ cages is apart from the other (Fig. 6(c), 6(d)). Moreover, the $5^{12}6^4$ cage in the CS-II hydrate is relatively isotropic and has nearly uniform center-to-host distance (4.59-4.69 Å for propane hydrate) [1,59], while the $5^{12}6^8$ cage in the HS-III shows a large discrepancy in the center-to-host distance (4.92-5.74 Å for methylcyclohexane+CH_4 hydrate) [1,60]. Therefore, it is expected that the Me_4N^+ cation in the OH^--incorporated CS-II hydrate interacts with more uniformly distributed surrounding anions at a shorter distance than the $Et_2Me_2N^+$ cation in the HS-III hydrate. This difference between Me_4NOH and Et_2Me_2NOH hydrates could cause the different trends of two hydrates in thermodynamic stability, as represented in Fig. 5.

For the fluoride-incorporated hydrates, the incorporation of fluoride instead of hydroxide causes inhibition of both the CS-II Me_4N^+ and the HS-III $Et_2Me_2N^+$ hydrate formation as shown in Fig. 5. In particular, the inhibition effect of fluoride incorporation on the CS-II hydrate (Fig. 5(a)) is much greater than on the HS-III hydrate (Fig. 5(b)). This could be due to the difference of large cages in size. As stated above, the filling space of fluoride in the lattice could be slightly larger, and thus the cage distortion caused by fluoride could also be slightly greater than by hydroxide. For huge, united cages of n-Bu_4NF and n-Bu_4NOH hydrates, the effect on thermodynamic stability caused by the difference between fluoride and hydroxide in space volume might be negligible, and the melting points of two hydrates are similar to each other [36]. On the other hand, for the 'relatively small' $5^{12}6^4$ cages of CS-II hydrate, the cage distortion by anion much affects the thermodynamic stability of the clathrate lattice, and this causes greater inhibition by the fluoride incorporation, as shown in Fig. 5(a). The $5^{12}6^8$ cage is larger than the $5^{12}6^4$ cage; thus, the incorporation of fluoride on HS-III hydrate 'less destabilizes' the hydrate lattice than on CS-II hydrate.

CONCLUSION

We have demonstrated that the fluoride ion can be incorporated in the CS-II and HS-III ionic clathrate hydrates. With the

Rietveld analysis of PXRD patterns, we identified the binary Me_4NF+N_2 or O_2 CS-II hydrates and Et_2Me_2NF+CH_4 HS-III hydrate. The phase equilibria of hydroxide or fluoride-incorporated CS-II and HS-III hydrates systems were also investigated, and it was confirmed that the incorporation of fluoride more destabilizes the hydrate lattice than that of hydroxide and that the degree of destabilization by fluoride might depend on the size of cages for the ionic guest species. The findings in this study may provide a better understanding of the guest–host interactions in ionic clathrate hydrates and contribute to their practical applications in gas storage and separation technologies.

ACKNOWLEDGEMENTS

The authors acknowledge the support by NRF Korea (2021R1 F1A1047221) funded by the Ministry of Science and ICT, Korea. The synchrotron PXRD experiments were carried out at Beamline 2D of the Pohang Accelerator Laboratory (PAL).

REFERENCES

1. J. A. Ripmeester, S. Takeya and S. Alavi, in *Clathrate hydrates: Molecular science and characterization*, J. A. Ripmeester and S. Alavi Eds., Wiley, Weinheim (2022).
2. G. A. Jeffrey, in *Inclusion compounds*, Vol. 1, J. L. Atwood, J. E. D. Davies and D. D. MacNicol Eds., Academic Press, London (1984).
3. D. W. Davidson and J. A. Ripmeester, in *Inclusion compounds*, Vol. 3, J. L. Atwood, J. E. D. Davies and D. D. MacNicol Eds., Academic Press, London (1984).
4. K. Koga, H. Tanaka and K. Nakanishi, *Mol. Simul.*, **12**, 241 (1994).
5. M. Cha, K. Shin and H. Lee, *Korean J. Chem. Eng.*, **34**, 2514 (2017).
6. H. Dureckova, T. K. Woo, S. Alavi and J. A. Ripmeester, *Can. J. Chem.*, **93**, 864 (2015).
7. H. Dureckova, T. K. Woo and S. Alavi, *J. Chem. Phys.*, **144**, 044501 (2016).
8. K. A. Udachin, S. Alavi and J. A. Ripmeester, *J. Phys. Chem. C*, **117**, 14176 (2013).
9. S. U. Pickering, *J. Chem. Soc. (London) Trans.*, **63**, 141 (1893).
10. K. Shin, J.-H. Cha, Y. Seo and H. Lee, *Chem. Asian. J.*, **5**, 22 (2010).
11. H. Bode and G. Teufer, *Acta Crystallogr.*, **8**, 611 (1955).
12. D. W. Davidson and S. K. Garg, *Can. J. Chem.*, **50**, 3515 (1972).
13. D. W. Davidson, L. D. Calver, F. Lee and J. A. Ripmeester, *Inorg. Chem.*, **20**, 2013 (1981).
14. D. Mootz, E. J. Oellers and M. Wiebcke, *J. Am. Chem. Soc.*, **109**, 1200 (1987).
15. J.-H. Cha, K. Shin, S. Choi, S. Lee and H. Lee, *J Phys. Chem. C*, **112**, 13332 (2008).
16. K. Shin, W. Lee, M. Cha, D.-Y. Koh, Y. N. Choi, H. Lee, B. S. Son, S. Lee and H. Lee, *J. Phys. Chem. B*, **115**, 958 (2011).
17. K. Shin, M. Cha, W. Lee and H. Lee, *Korean J. Chem. Eng.*, **33**, 1728 (2016).
18. D. Mootz and R. Seidel, *J. Incl. Phenom.*, **8**, 139 (1990).
19. S. Choi, K. Shin and H. Lee, *J. Phys. Chem. B.*, **111**, 10224 (2007).
20. K. Shin, S. Choi, J.-H. Cha and H. Lee, *J. Am. Chem. Soc.*, **130**, 7180 (2008).
21. K. Shin, M. Cha, S. Choi, J. Dho and H. Lee, *J. Am. Chem. Soc.*, **130**, 17234 (2008).
22. M. Cha, K. Shin, M. Kwon, D.-Y. Koh, B. Sung and H. Lee, *J. Am. Chem. Soc.*, **132**, 3694 (2010).
23. K. Shin, M. Cha, H. Kim, Y. Jung, Y. S. Kang and H. Lee, *Chem. Commun.*, **47**, 674 (2011).
24. K. Shin, M. Cha, W. Lee, H. Kim, Y. Jung, J. Dho, J. Kim and H. Lee, *J. Am. Chem. Soc.*, **133**, 20399 (2011).
25. K. Shin, M. Cha, W. Lee, Y. Seo and H. Lee, *J. Phys. Chem. C*, **118**, 15193 (2014).
26. Y.-H. Ahn, D. Lim, J. Min, J. Kim, B. Lee, J. W. Lee and K. Shin, *Chem. Eng. J.*, **359**, 1629 (2019).
27. D. L. Fowler, W. V. Loebenstein, D. B. Pall and C. A. Kraus, *J. Am. Chem. Soc.*, **62**, 1140 (1940).
28. W. Shimada, M. Shiro, H. Kondo, S. Takeya, H. Oyama, T. Ebinuma and H. Narita, *Acta. Crystallogr. C*, **C61**, 065 (2005).
29. K. Shin, Y. Kim, T. A. Strobel, P. S. R. Prasad, T. Sugahara, H. Lee, E. D. Sloan, A. K. Sum and C. A. Koh, *J. Phys. Chem. A*, **113**, 6415 (2009).
30. J.-H. Cha, K. Shin, S. Choi and H. Lee, *J. Phys. Chem. C*, **112**, 10573 (2008).
31. S. Muromachi, K. A. Udachin, K. Shin, S. Alavi, I. L. Moudrakovski, R. Ohmura and J. A. Ripmeester, *Chem. Commun.*, **50**, 11476 (2014).
32. B. Lee, K. Shin, S. Muromachi, I. L. Moudrakovski, C. I. Ratcliffe and J. A. Ripmeester, *Chem. Eng. J.*, **418**, 129304 (2021).
33. H. Hashimoto, T. Yamaguchi, H. Ozeki and S. Muromachi, *Sci. Rep.*, **7**, 17216 (2017).
34. H. Hashimoto, H. Ozeki, Y. Yamamoto and S. Muromachi, *ACS Omega*, **5**, 7115 (2020).
35. T. Kobori, S. Muromachi, T. Yamasaki, S. Takeya, Y. Yamamoto, S. Alavi and R. Ohmura, *Cryst. Growth Des.*, **15**, 3862 (2015).
36. H. Nakayama and S. Torigata, *Bull. Chem. Soc. Jpn.*, **57**, 171 (1984).
37. K. Shin, I. L. Moudrakovski, M. D. Davari, S. Alavi, C. I. Ratcliffe and J. A. Ripmeester, *CrystEngComm*, **16**, 7209 (2014).
38. K. Shin, I. L. Moudrakovski, C. I. Ratcliffe and J. A. Ripmeester, *Angew. Chem. Int. Ed.*, **56**, 6171 (2017).
39. B. Lee, J. Kim, K. Shin, K. H. Park, M. Cha, S. Alavi and J. A. Ripmeester, *CrystEngComm*, **23**, 4708 (2021).
40. J. Kim, B. Lee, K. Shin, S.-P. Kang K. H. Park, M. Cha, S. Alavi and J. A. Ripmeester, *Ind. Eng. Chem. Res.*, **60**, 11267 (2021).
41. J. Kim, K. Shin, S. Alavi and J. A. Ripmeester, *Energy Fuels*, **36**, 10504 (2022).
42. B. Lee, K. Shin, S. Alavi and J. A. Ripmeester, *Energy Fuels*, **36**, 11123 (2022).
43. S. Zaromb and R. J. Brill, *J. Chem. Phys.*, **24**, 895 (1956).
44. L. C. Labowitz and E. F. Westrum, *J. Phys. Chem.*, **65**, 408 (1961).
45. C. G. van Beek, J. Overeem, J. R. Ruble and B. M. Craven, *Can. J. Chem.*, **74**, 943 (1996).
46. K. Shin, I. L. Moudrakovski, K. A. Udachin, C. I. Ratcliffe and J. A. Ripmeester, *Can. J. Chem.*, **93**, 850 (2015).
47. S. Takeya, K. A. Udachin, I. L. Moudrakovski, R. Susilo and J. A. Ripmeester, *J. Am. Chem. Soc.*, **132**, 524 (2010).
48. F. Favre-Nicolin and R. Cerny, *J. Appl. Crystallogr.*, **35**, 734 (2002); R. Cerny and F. Favre-Nicolin, *Z. Kristallogr.*, **222**, 105 (2007).
49. J. Rodríguez-Carvajal, *Phys. B Condens. Matter*, **192**, 55 (1993).
50. K. Momma and F. Izumi, *J. Appl. Crystallogr.*, **44**, 1272 (2011).
51. R. D. Shannon, *Acta Cryst.*, **A32**, 751 (1976).

52. F. J. Millero, *Chem. Rev.*, **71**, 147 (1971).
53. Y. Marcus, *J. Phys. Chem. B*, **113**, 10285 (2009).
54. Y. Marcus, *J. Chem. Phys.*, **137**, 154501 (2012).
55. A. H. Mohammadi and D. Richon, *Ind. End. Chem. Res.*, **49**, 3976 (2010).
56. A. Van Cleeff and G. A. M. Diepen, *Rec. Trav. Chim.*, **84**, 1085 (1965).
57. A. Van Cleeff and G. A. M. Diepen, *Rec. Trav. Chim.*, **79**, 582 (1960).
58. A. H. Mohammadi, R. Anderson and B. Tohidi, *AIChE J.*, **51**, 2825 (2005).
59. K. A. Udachin, H. Lu, G. D. Enright, C. I. Ratcliffe, J. A. Ripmeester, N. R. Chapman, M. Riedle and G. Spence, *Angew. Chem. Int. Ed.*, **46**, 8220 (2007).
60. K. A. Udachin, C. I. Ratcliffe and J. A. Ripmeester, *J. Supramol. Chem.*, **2**, 405 (2002).